Geophysical Research Letters

RESEARCH LETTER
10.1029/2022GL101155

Superstoichiometric Alloying of H and Close-Packed Fe-Ni Metal Under High Pressures: Implications for Hydrogen Storage in Planetary Core

Hélène Piet[1], Andrew Chizmeshya[2], Bin Chen[3], Stella Chariton[4], Eran Greenberg[4,5], Vitali Prakapenka[4], Peter Buseck[1,2], and Sang-Heon Shim[1]

[1]School of Earth and Space Exploration, Arizona State University, Tempe, AZ, USA, [2]School of Molecular Sciences, Arizona State University, Tempe, AZ, USA, [3]Hawaii Institute of Geophysics and Planetology, University of Hawaii at Manoa, Honolulu, HI, USA, [4]Center for Advanced Radiation Sources, University of Chicago, Chicago, IL, USA, [5]Now at Soreq Nuclear Research Center, Applied Physics Department, Yavne, Israel

Key Points:

- Iron-nickel alloy quenched from liquid at high pressures contains more than 3.1 wt% hydrogen
- Liquid iron-nickel alloy can contain at least 80% more H than the solid
- Hydrogen storage capacity of the liquid part of the core could be the largest among the internal layers of planets

Supporting Information:

Supporting Information may be found in the online version of this article.

Correspondence to:

S.-H. Shim,
sshim5@asu.edu

Citation:

Piet, H., Chizmeshya, A., Chen, B., Chariton, S., Greenberg, E., Prakapenka, V., et al. (2023). Superstoichiometric alloying of H and close-packed Fe-Ni metal under high pressures: Implications for hydrogen storage in planetary core. *Geophysical Research Letters*, *50*, e2022GL101155. https://doi.org/10.1029/2022GL101155

Received 4 SEP 2022
Accepted 18 FEB 2023

Author Contributions:

Conceptualization: Hélène Piet, Sang-Heon Shim
Data curation: Hélène Piet
Formal analysis: Hélène Piet, Andrew Chizmeshya, Sang-Heon Shim
Funding acquisition: Peter Buseck, Sang-Heon Shim
Investigation: Hélène Piet, Andrew Chizmeshya, Sang-Heon Shim
Methodology: Andrew Chizmeshya, Stella Chariton, Eran Greenberg, Vitali Prakapenka
Project Administration: Sang-Heon Shim
Supervision: Sang-Heon Shim

Abstract

Although high pressure enables alloying between hydrogen and iron, hydrogen-to-iron molar ratio (H/Fe) so far found in experiments is mostly limited to 1 in the close-packed iron metal under high pressure. We report a H/(Fe + Ni) ratio of 1.8 ± 0.1 from $(Fe,Ni)H_x$ (or $x \geq 1.8$) quenched from liquid, exceeding the amounts so far reported for densely packed Fe alloys. From the metastable behavior of the frozen $(Fe,Ni)H_x$ liquid during decompression, we infer that the amount is a lower bound and therefore even a greater amount of H can be dissolved in the liquid part of Fe-rich cores of planets. The significant H storage capacity of liquid Fe-Ni alloy is important to consider for potential storage of H in the interiors of low-density planets as well as rocky planets.

Plain Language Summary

Our new high-pressure experiments show that much more hydrogen can dissolve in the iron-nickel alloy liquid than what is known for solid iron-nickel alloy at high pressures and high temperatures. These experimental observations open up the possibility for large internal hydrogen storage in the metallic cores for a range of planet types.

1. Introduction

The Earth's core is primarily composed of Fe alloyed with ~5.5 wt.% Ni (McDonough, 2003). The observed density deficit suggests a considerable amount of light elements in the core (Birch, 1964). Hydrogen has been considered as one of the light element candidates (Poirier, 1994). Despite its dominance in planetary systems, however, the effects of hydrogen are not well understood because of experimental challenges associated with its study at high pressure–temperature (*P-T*). Thanks to recent technical advances, such as pulsed laser heating with gated X-ray diffraction (Deemyad et al., 2005; Goncharov et al., 2010), and an evolving vision of the important role of hydrogen in the dynamics and compositions of the interiors of a wide range of planets (Seager & Deming, 2010), the last decade has seen a surge in studies of the Fe–H system under high *P-T* conditions (Ikuta et al., 2019; Kato et al., 2020; Narygina et al., 2011; Ohta et al., 2019; Pépin et al., 2014, 2017; Shibazaki et al., 2014; Tagawa et al., 2022; Thompson et al., 2018). These studies have documented the stability of face-centered cubic structured (fcc) FeH_x at 10–137 GPa. However, in these studies, it appears that H solubility in close-packed FeH_x is limited to $x \leq 1$. On the other hand, a series of polyhydrides have also been found in which H/Fe molar ratio increases with increasing pressure: FeH_2 at 67 GPa, FeH_3 at 86 GPa, and FeH_5 at ≥130 GPa (Pépin et al., 2014, 2017). However, the polyhydrides were all synthesized at temperatures much lower (500–1500 K) than those expected for planetary interiors and some theoretical studies predict the close-packed structured Fe-H alloys as the most stable form up to 400 GPa (Sagatova et al., 2020).

While liquid Fe-Ni alloy of the outer core may contain more light elements than the inner core, it is unknown if the solubility of hydrogen in the liquid alloy is higher than the solid. There have been a number of measurements to study H solubility in Fe metal. However, most of them did not reach high enough temperatures expected for Fe-Ni liquid stability and therefore the outer core (at least 1800 K or higher). Also, while a pure source for hydrogen is desirable for clear understanding of H effects, most studies have used hydrogen sources with other elements, such as paraffin (C_nH_n) and water (H_2O). Because these other elements can alloy with Fe metal, it is difficult to isolate the effects of hydrogen and therefore pure H_2 is desirable (Tagawa et al., 2016). The main reason for this

Validation: Hélène Piet
Visualization: Hélène Piet, Andrew Chizmeshya, Sang-Heon Shim
Writing – original draft: Hélène Piet, Andrew Chizmeshya, Sang-Heon Shim
Writing – review & editing: Andrew Chizmeshya, Sang-Heon Shim

experimental design is because when pure hydrogen is used as a medium H_2 can diffuses into the diamond anvils, causing them to fail, particularly at temperatures relevant for melting of metals and silicates. Here, we report the solubility of hydrogen in metallic iron-nickel alloy frozen from liquid up to 77 GPa in the laser-heated diamond anvil cell (LHDAC). We mitigate the H diffusion problems using the gold coating of gaskets (Pépin et al., 2014) and pulsed-laser heating (Deemyad et al., 2005). We also discuss the implications of the increased solubility of H for the cores of planets.

2. Methods

2.1. High-Pressure Experiments

Two different starting materials were used: pure metallic iron (reagent grade powder from Alfa Aesar), and metallic Fe-6.5(4)%Ni (see Text S1 in Supporting Information S1 for synthesis method). The metal samples were stored in a vacuum chamber and possible oxidation was examined by Raman and XRD before loading. We compressed the sample in diamond-anvil cells (DACs), with diamond culet sizes ranging between 200 and 150 μm. We drilled the sample chamber (approximately 70% of the culet size) in a pre-compressed rhenium gasket, which we later coated with gold (≥80 Å in thickness) to prevent embrittlement by hydrogen during experiments (Pépin et al., 2014). We loaded the sample as a foil into the sample chamber, which was propped on both sides by pieces of the same material to avoid full contact with the anvils and provide better laser coupling during heating. The foil was made by compressing 1 μm grain size powder in a DAC. The thickness of the foil was approximately 5 μm. We loaded a piece of ruby and a piece of gold for pressure measurement (Ye et al., 2017). These grains were loaded apart from the sample to avoid contamination during laser heating. Pure hydrogen gas was then loaded into the sample chamber using a loading system at Arizona State University. The sample chamber decreases after loading approximately by 30%–40% because of high compressibility of a hydrogen medium.

We acquired X-ray diffraction (XRD) patterns at high pressures in LHDAC at the 13-IDD beamline of the GSECARS sector of the Advanced Photon Source (Table S1 in Supporting Information S1). A 3×4 μm^2 monochromatic X-ray beam with energy of 30 keV or 37 keV was co-axially aligned with double-sided near-infrared laser-heating beam providing a 15 μm-diameter heating spot. The laser pulse (1 μs pulses) is synchronized with gated X-ray and temperature detectors to allow XRD acquisition at in situ high P-T (Goncharov et al., 2010). To monitor the sample through XRD during heating, we generate a series of 10^5 pulses to a repetition rate of 10 kHz and accumulate the obtained diffraction patterns. After heating at 300 K, we measured XRD without gating. The temperature is calculated by fitting a Planck equation to the thermal radiation spectra collected on both sides of the DAC assuming a gray-body approximation. We collected 2D diffraction images using a Pilatus 1M CdTe detector. We used a LaB_6 standard to calibrate and correct distortions and detector distance (~200 mm) during integration from 2D images to 1D patterns in the Dioptas software (Prescher & Prakapenka, 2015). We used the PeakPo software package (Shim, 2017) for peak identification and unit-cell fitting. Rietveld refinements were performed on selected diffraction patterns in GSAS-II package (Toby & Von Dreele, 2013).

2.2. Density Functional Theory (DFT) Calculations

The DFT calculations in this study enable us to understand how different amounts of H change the unit-cell volume of fcc FeH_x alloy and then apply that knowledge to calculate the amount of H in the alloys observed in our experiments based on their expansion of unit-cell volumes. All spin-density functional calculations on the FeH_x (x = 0–3) systems were carried out using the Vienna Ab initio Simulation Package (VASP) code (Kresse & Furthmüller, 1996) and the Perdew-Burke-Ernzerhof (PBE) version of generalized gradient approximation (GGA) for exchange and correlation (Perdew et al., 1996). Core state were treated using the projector augmented wave (PAW) (Kresse & Joubert, 1999) method in which H [$1s^1$] and Fe [$2p^6 3d^7 4s^1$] electrons were explicitly treated. A plane-wave basis with an energy cutoff of 500 eV in combination with $16 \times 16 \times 16$ Monkhorst-Pack k-point grids led to energy, force and stress convergence of 0.1 meV, 10^{-5} eV/A, and 0.1 kbar, respectively. Thorough structure optimizations were first performed on all systems in the static lattice approximation (no zero-point energy or thermal corrections). Accurate compression equations of state (EOS) were obtained using the isochoric approach, in which the static-lattice energy is evaluated over a range of volumes (typically 20) surrounding the static-lattice minimum, including several expanded structures. At each volume the shape and internal atomic positions are fully optimized, yielding an energy-volume data set which was then fit to third order

Birch-Murnaghan form (Birch, 1947) to obtain the static-lattice ground state energy, volume, bulk modulus and bulk modulus derivative at $P = 0$. The magnetization of the system was also carefully analyzed at each volume to establish magnetic state, and identify magnetic phase changes.

In fcc FeH_x, H can be hosted in the octahedral and the tetrahedral sites. Different site occupancies for H were therefore investigated (Table S2 in Supporting Information S1). We also considered different magnetic states (ferromagnetic (FM) and antiferromagnetic (AFM)) and extracted the corresponding magnetic moment (μ). While a range of possibility exists for AFM ordering, for the sake of simplicity, we consider alternating spin directions along the c axis of the fcc lattice (see Text S2 in Supporting Information S1). We calculated the compression of these phases at 0 K and up to 190 GPa.

An additional calculation was conducted to explore the influence of Ni incorporation into $FeH_{1.5}$. We first built a structure model with a rhombohedral supercell containing eight Fe sites and 12 tetrahedrally coordinated H atoms. A single Ni atom was then placed on the (1/2 1/2 1/2) position at the center of the cell to yield a system with composition Fe_7NiH_{12} or $(Fe_{0.875}Ni_{0.125})H_{1.5}$. The pressure dependence of the thermodynamic stability of these alloys were estimated by calculating their static formation enthalpies (H) relative to fcc Ni, orthorhombic solid H_2 ($C2/c$ structure) and both fcc Fe and hcp Fe according to:

$$\Delta H(\mathrm{Fe_{0.875}Ni_{0.125}H_{1.5}}) = H(\mathrm{Fe_{0.875}Ni_{0.125}H_{1.5}}) - 0.875H(\mathrm{Fe}) - 0.125H(\mathrm{Ni}) - \frac{3}{4}H(\mathrm{H_2}). \tag{1}$$

The formation enthalpy can also be computed relative to iron and nickel hydrides provided the pressure dependence of all phases is known:

$$\begin{aligned}\Delta H_{hyd}(\mathrm{Fe_{0.875}Ni_{0.125}H_{1.5}}) = H(\mathrm{Fe_{0.875}Ni_{0.125}H_{1.5}}) - 0.875H(\mathrm{FeH_{1.5}})\\ - 0.125H(\mathrm{NiH_{1.5}}).\end{aligned} \tag{2}$$

While the EOS of Fe_2H_3 ($FeH_{1.5}$) is well-established, the corresponding data for Ni_2H_3 has only recently been reported (Binns et al., 2018; Ying et al., 2018). The formation enthalpy of the nickel hydride relative to elements is:

$$\Delta H(\mathrm{NiH_{1.5}}) = H(\mathrm{NiH_{1.5}}) - H(\mathrm{Ni}) - \frac{3}{4}H(\mathrm{H_2}), \tag{3}$$

which has recently been calculated at 60 GPa where a stable $C2/c$ structure has been observed (Binns et al., 2018; Ying et al., 2018). The formation enthalpy relative to elements, $\Delta H(Fe_{0.875}Ni_{0.125}H_{1.5})$, and Fe/Ni hydrides, $\Delta H_{hyd}(Fe_{0.875}Ni_{0.125}H_{1.5})$, are related according to:

$$\begin{aligned}\Delta H(\mathrm{Fe_{0.875}Ni_{0.125}H_{1.5}}) &= H(\mathrm{Fe_{0.875}Ni_{0.125}H_{1.5}}) - 0.875H(\mathrm{Fe}) - 0.125H(\mathrm{Ni}) - \frac{3}{4}H(\mathrm{H_2})\\ &= \Delta H_{hyd}(\mathrm{Fe_{0.875}Ni_{0.125}H_{1.5}}) + 0.875\Delta H(\mathrm{FeH_{1.5}})\\ &\quad + 0.125\Delta H(\mathrm{NiH_{1.5}}).\end{aligned} \tag{4}$$

The same computational parameters as described above were used in the PAW-GGA calculations of all required phases. For Ni, 16 valence electrons were explicitly treated using PAW pseudopotentials with a cutoff of 368 eV. Full spin-density and structure optimization was carried out from 0 to 100 GPa in steps of 10 GPa (see Text S3 in Supporting Information S1 for detail).

3. Results and Discussion

3.1. In Situ X-Ray Diffraction Experiments

At lower pressures (26 GPa), our results for the Fe–H system are largely consistent with previous reports (Badding et al., 1991; Kato et al., 2020; Narygina et al., 2011; Pépin et al., 2014; Thompson et al., 2018): (a) formation of dhcp FeH_x (dhcp: double hexagonal close packed) by compression of metallic Fe in a H medium at 300 K, and (b) formation of fcc FeH_x upon heating to temperatures above 1160 K. The unit-cell volumes of dhcp and fcc FeH_x measured after synthesis (Table S1 in Supporting Information S1) also agree with previous reports at this pressure range where the magnitude of volume increase found in the phases was interpreted to be consistent with $x = 1$ in FeH_x.

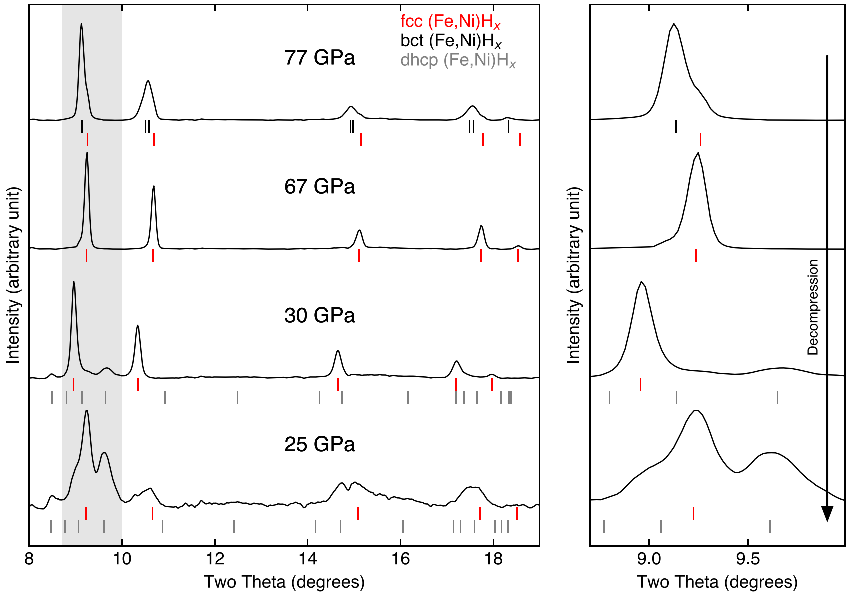

Figure 1. X-ray diffraction patterns measured at high pressures and 300 K after laser heating at 77 GPa and 2720 ± 150 K. The *d*-spacings of the fcc (Fe,Ni)H_x peak anomalously decreases from 77 to 67 GPa, followed by a "normal" gradual increase in *d*-spacing from 67 to 30 GPa and an abrupt shift to a lower *d*-spacing at 30 GPa. The *d*-spacings of the fcc (Fe,Ni)H_x experiences an abrupt shift to a lower *d*-spacing at 25–30 GPa. Below 25 GPa, the peak shifts show expected behavior until the phase converts to bcc Fe by H loss upon quenching to 1 bar. The right panel shows shifts of the 111_{fcc} and 101_{bct} peaks (the gray rectangular area in the left panel). X-ray wavelength was 0.3344 Å.

While enabling heating of the samples in a H medium to very high temperatures, a pulse heating run involves integration of thousands of short heating events (Deemyad et al., 2005; Goncharov et al., 2010). Despite the difference in time duration and heating style, the phase behavior of the Fe-H system agrees well with those previously reported with different heating methods and hydrogen sources at the overlapping *P-T* ranges (Kato et al., 2020; Narygina et al., 2011; Thompson et al., 2018). Therefore, the pulse heating method in this study does not affect the results and provides results consistent with continuous laser heating. A recent study found consistent results between pulsed and continuous laser heating on Fe-Si alloy in a H medium in LHDAC (Fu et al., 2023).

We conducted similar experiments at higher pressures (Figure 1). After heating to 2720 K at 77 GPa, we found clear sign of melting in optical imaging of the sample (Figure 6 in Piet et al. (2021)). In fact, the temperature is 400–700 K higher than estimated melting temperature of FeH_x (Hirose et al., 2019; Sakamaki et al., 2009). We note that a small amount of Ni does not change the melting temperature of Fe significantly (Zhang et al., 2016). After temperature quenching to 300 K at 77 GPa, the diffraction patterns are consistent with that expected for the fcc structure, while we did not find any evidence for tetragonal FeH_2 documented at the pressure range with lower-temperature heating (Pépin et al., 2017). The diffraction peaks of fcc (Fe,Ni)H_x shifted to lower angles much more than expected from previous studies, indicating much larger volume than any of the previous reports (Figure 2).

Previous experimental studies have estimated the H content of synthesized FeH_x phases (x) from the volume difference between close-packed structured FeH_x and Fe metal,

$$x = \frac{V(\mathrm{FeH}_x) - V(\mathrm{Fe})}{\Delta V_{\mathrm{H}}}, \tag{5}$$

assuming that the volume increase by H (ΔV_{H}) is proportional to the H content (x). The volume increase, $\Delta V = V(\mathrm{FeH}_x) - V(\mathrm{Fe})$, per Fe after melting at 77 GPa is 3.33 Å^3 when the diffraction pattern was fit to an fcc structure and V(Fe) is taken from the equation of state of fcc Fe from Dorogokupets et al. (2017). Note that Ni has little effect on the unit-cell volume of Fe-Ni alloys when Ni content is low (Mao et al., 2006), which is the case for our sample. For the range of $\Delta V_{\mathrm{H}} = 1.9 - 2.2$ Å^3/H considered in the literature (Antonov et al., 2019; Ikuta

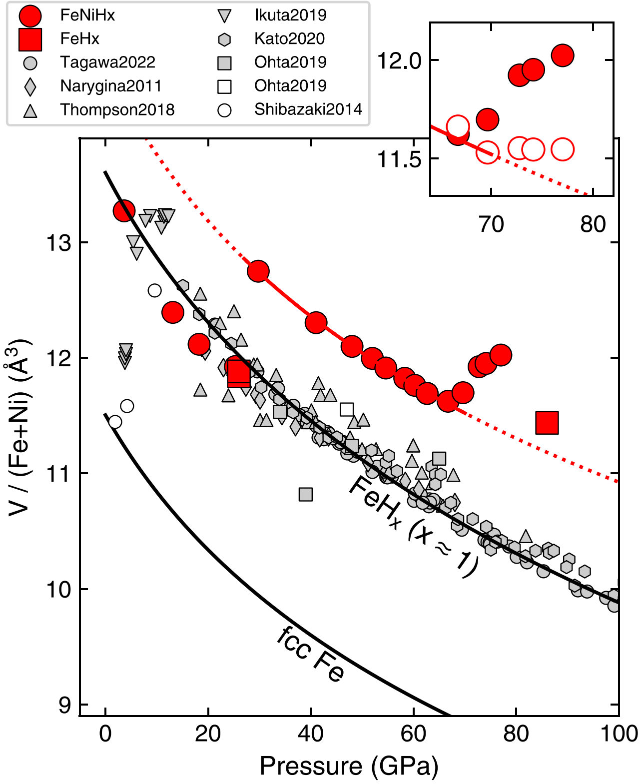

Figure 2. Volume per Fe + Ni atom observed in this study (red squares for fcc FeH_x and red circles for fcc $(Fe,Ni)H_x$) compared with those from previous studies (Ikuta et al., 2019; Kato et al., 2020; Narygina et al., 2011; Ohta et al., 2019; Shibazaki et al., 2014; Tagawa et al., 2022; Thompson et al., 2018) (gray symbols for fcc FeH_x and open symbols for fcc $(Fe,Ni)H_x$). The equation of state for fcc Fe (H/Fe = 0) and fcc FeH (H/Fe = 1) are from Dorogokupets et al. (2017) and Kato et al. (2020), respectively. The red curve is a guide for eye for our data points. The inset shows the volumes measured above 70 GPa where the diffraction patterns were fit to a two phase model: bct (solid red) + fcc (open red) (see text for details). The decompression data for $(Fe,Ni)H_x$ was obtained for the sample synthesized at 77 GPa in Piet et al. (2021). All three data points for FeH_x are obtained after all three separate heating runs.

et al., 2019; Narygina et al., 2011), the volume measured at 77 GPa after melting yields $x = 1.51 - 1.74$ for $(Fe,Ni)H_x$.

The XRD patterns show some peak splitting and broadening at 77 GPa after melting (Figure 1), indicating either a distortion of the fcc structure (such as to a body-centered tetragonal structure, bct) or the existence of more than one fcc phase. Our DFT calculations (described later) predict that some distortions in fcc Fe-H alloy could result in a bct structure (Table S2 in Supporting Information S1). We conducted Rietveld refinements using three models: (a) a single fcc phase, (b) a mixture of bct + fcc and (c) a mixture of two fcc phases. The observed broadening of the $111_{\rm fcc}$ peak indicates that a single bct phase is unlikely to explain the distortion since this peak does not show splitting in bct. Rietveld refinement for the bct + fcc model yields the lowest R_{wp} value at 0.30% (Figure S1 in Supporting Information S1). The bct phase is dominant with a phase fraction of 92 vol% (Table S3 in Supporting Information S1). The bct distortion may result from a large amount of H in the crystal. The volume of bct is nearly identical to the value we obtained when single fcc phase was assumed for the fitting and therefore the estimated value of x between 1.51 and 1.74, unaffected by different fitting strategy. In this case, because bct does not deviate significantly from fcc, we assumed that volume behavior of bct remains comparable to that of fcc. For the minor fcc phase, the same estimation yields $x = 1.30 - 1.51$. Therefore, regardless of the fit models, hydrogen content (x) is much greater than previously reported ($x \approx 1$). It is possible that the local difference in temperature quench rate contributed to the different amount of H preserved in the solid frozen from liquid.

We also observed an unusually large unit-cell volume for thermally quenched fcc FeH_x at 89 GPa without Ni. The observed volume increase yields $x = 1.35 - 1.56$ for the empirical $\Delta V_{\rm H}$ values. However, unlike the Ni-bearing case, we do not observe peak splitting and broadening, and the diffraction patterns are consistent with a single fcc phase, which may indicate that bct distortion only appears when H/Fe is sufficiently large ($x > 1.5$). From these observations and comparisons, we interpret that the significant volume expansion beyond what is expected for H/Fe = 1 above 77 GPa is due to increased H solubility in $(Fe,Ni)H_x$ liquid. The reason previous studies did not observe the large H solubility is likely because their synthesis temperatures were not high enough for melting (the data points we report here are from the samples synthesized in Piet et al. (2021)).

Another set of evidence supporting the argument that the super-stoichiometric H content of our $(Fe,Ni)H_x$ samples is from liquid was found during decompression measurements at 300 K (Figure 2; data are provided in Table S1 in Supporting Information S1). Upon decompression from the synthesis pressure (77 GPa) down to 70 GPa, we observed a steady *decrease* in the unit-cell volumes of $(Fe,Ni)H_x$, which is the opposite to the expected behavior of crystalline solids under decompression, that is, volume *increase* (insets in Figures 1 and 2). During decompression, the bct distortion also decreases whereas the fraction of the fcc phase increases (Table S3 in Supporting Information S1). This anomalous behavior can be best explained by the gradual loss of hydrogen with decreasing pressure, because the amount of H in the $(Fe,Ni)H_x$ sample exceeds the H storage capacity of the solid fcc phase. At 67 GPa, peaks are sharper (Figure 1) and almost no peak splitting is observed, consistent with the existence of a single fcc phase.

From 67 GPa down to 30 GPa, the unit-cell volume of the fcc phase remains anomalously high and the volume indicates $x = 1.25 - 1.45$ for empirical $\Delta V_{\rm H}$ values, but its decompression behavior appears to be normal. At 30 GPa, the dhcp phase appears in the diffraction patterns. At 25 GPa, the unit-cell volume of the fcc phase drops abruptly to the level expected for $x \approx 1$, again indicating another H loss of the sample at this pressure. From 25 GPa down to 4 GPa, we observe a gradual increase in the unit-cell volumes of the fcc and dhcp phases and the measured unit-cell volumes of the dhcp and fcc phases agree with those reported for $x \approx 1$ (Narygina

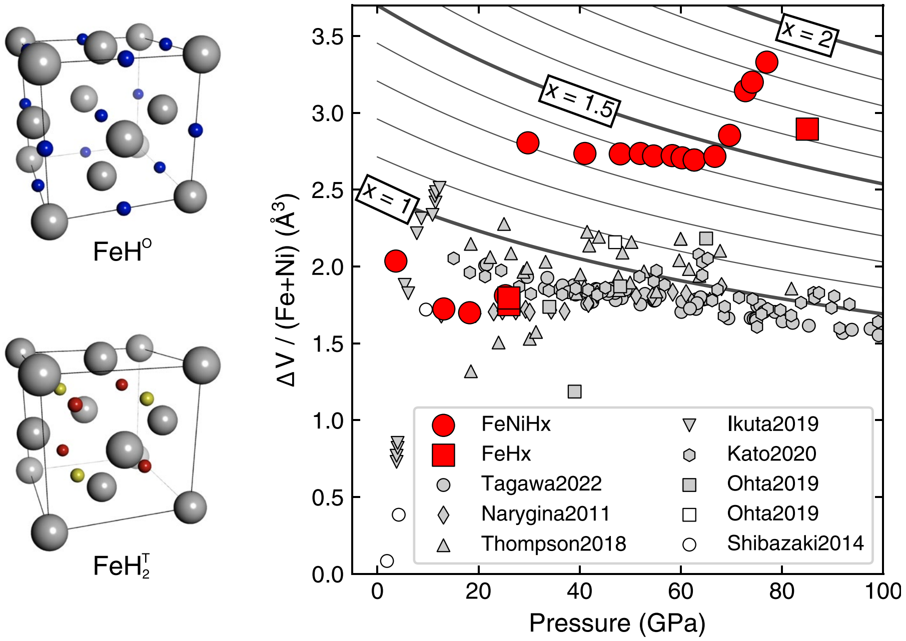

Figure 3. Volume increase by H incorporation, ΔV, observed for this study and other studies (data points; notations are the same as Figure 2) compared with ΔV from our DFT results for different amount of H (contour lines). ΔV was calculated from: $V_{\text{obs}} - V(\text{Fe})$ where V_{obs} is the observed volume for FeH_x and $V(\text{Fe})$ is the volume of H-free fcc Fe calculated using EOS of Dorogokupets et al. (2017). The contours are estimated by taking difference in volume between fcc FeH_3 ($V_0 = 18.043$ Å^3, $K_0 = 179.3$ GPa, and $K_0' = 4.26$ in Vinet equation) and fcc Fe ($V_0 = 10.644$ Å^3, $K_0 = 172.4$ GPa, and $K_0' = 6.91$ in Vinet equation) from our DFT calculations: $1/3 \times (V(\text{FeH}_3) - V(\text{Fe})) \times x$. On the left side, crystal structures of fcc FeH_x with H in all octahedral sites, FeH^{O}, and H in all tetrahedral sites, FeH_2^{T}, are shown. The red spheres in FeH_2^{T} highlight the arrangement of H atoms in a tetrahedral motif which is considered for partial occupancy of H atoms in FeH^{T}.

et al., 2011; Pépin et al., 2014). The behaviors we observed here indicates that the H content in the crystalline phase quenched from liquid ($x \gg 1$) is beyond the H amount a stable fcc $(\text{Fe,Ni})\text{H}_x$ can store. Therefore, H gradually escapes from the crystalline phase quenched from liquid with decompression as it becomes further destabilized by decompression.

3.2. Hydrogen Content of the Fe-Ni-H Phases

A conventional 4-atom fcc cell contains 12 interstitial sites (four octahedral and eight tetrahedral sites) where H can be hosted (Figure 3). H/Fe ratios in a fcc cell can therefore range anywhere from 0 up to 3 and H/Fe (or x) > 1 requires some level of H occupancy in the tetrahedral sites. The incorporation of H into the interstitial sites leads to an expansion of the fcc structure and therefore an increase of its volume with respect to that of H-free fcc Fe.

The empirical method of estimating H content from the volume increase used in the previous section and the previous studies comes with two sources of significant uncertainty: (a) can ΔV_{H} be pressure dependent? and (b) can ΔV_{H} be different depending on whether H enters the octahedral or the tetrahedral site? For $(\text{Fe,Ni})\text{H}_x$, ΔV_{H} has been measured only up to 12 GPa (Ikuta et al., 2019). Impact of H on the compressibility of Fe alloy can be small if H content (x) is small, but for a system with a large amount of H, which is the case for the samples in this study, H could alter the compressibility of Fe alloy. The observed volume above 30 GPa is beyond the capacity of the octahedral interstitial site of the fcc structure (H/Fe = 1), meaning that the tetrahedral occupancy is important to consider. Studies have suggested that ΔV_{H} can be significantly different between the octahedral and the tetrahedral sites (Antonov et al., 2019; Ikuta et al., 2019).

In order to address these questions, we performed a series of DFT calculations. Ni itself has little effect on the unit-cell volume of Fe-Ni alloys with relatively low-Ni contents (Mao et al., 2006). Our DFT calculation for superstoichiometric $\text{FeH}_{1.5}$ and $(\text{Fe,Ni})\text{H}_{1.5}$ (described later in this section) found that the volume of the two phases is essentially the same (Table S4 in Supporting Information S1). Therefore, we conducted DFT calculation for FeH_x to estimate ΔV_{H}. We consider H/Fe ratios (or x in $(\text{Fe,Ni})\text{H}_x$) between 0 and 3 by using a range of different vacancy configurations (Figure 3): H in octahedral sites (H^{O}), in tetrahedral sites (H^{T}) and with mixed occupancy (H^{OT} or H^{TO} with dominantly occupied octahedral or tetrahedral sites, respectively). The DFT calculation shows that ΔV_H is pressure dependent in all the models we consider and it decreases with pressure, meaning that H makes Fe-Ni alloys more compressible (Table S2 in Supporting Information S1). Therefore, the assumption of a constant ΔV_H likely underestimates the amount of H in (Fe,Ni)H_x at high pressures, as used ΔV_H values are from measurements at pressures less than 12 GPa.

For H/Fe = 1, a model with all H atoms in octahedral sites (FM-FeH^{O}-LP) has a lower free-energy than with all H in tetrahedral sites (FM-FeH^{T}), suggesting that H preferentially enters the octahedral sites in a low-H regime. This result supports the existing view on H substitution in the close-packed structure of iron metal (Antonov, 2002). The magnetic moment of the FM-FeH^{O} model decreases with increasing pressure, becoming zero at 34 GPa. Above 34 GPa, however, non-magnetic (NM) FeH^{O}-HP becomes the lowest energy configuration.

For H/Fe = 1.5, models with full octahedral occupancy and partial tetrahedral occupancy ($FeH_{1.5}^{OT}$) yield lower energies than a model with all H in the tetrahedral sites ($FeH_{1.5}^{T}$), consistent again with the notion that H atoms would fill the octahedral sites first. H/Fe = 2 models in which all eight tetrahedral sites are occupied (FeH_2^{T}) possess a lower energy than models with fully occupied octahedral sites and partially occupied tetrahedral sites (FeH_2^{OT}). Therefore, H in the tetrahedral sites may become energetically competitive with an increase in H/Fe.

Because the sizes of the octahedral and the tetrahedral interstitial sites of fcc are different, ΔV_H is likely different for these two sites as also pointed out by Antonov et al. (2019). From the trend found in other 3*d* transition metal hydrogen alloys with well-characterized site occupancies, Antonov et al. (2019) predicted 1.9 Å^3/H and 3.1 Å^3/H for the ΔV_H's of the octahedral and the tetrahedral sites in FeH_x, respectively. Our DFT for $x = 1$ in FeH_x with all H in the octahedral sites found $\Delta V_H = 1.54$ Å^3/H at 0 GPa, somewhat lower than the value proposed for the same site by Antonov et al. (2019). The ΔV_H for the tetrahedral site found to be 3.08 Å^3/H in the FeH_2^{T} model, which agrees well with the estimation by Antonov et al. (2019) for the same site. The agreement is not surprising in that Antonov et al. (2019)'s estimation is from CoH_2 and CrH_2 where all H atoms are in the tetrahedral sites. However, it is difficult to take into account the octahedral and tetrahedral site effects separately in the case of FeH_x because H begins to enter the tetrahedral interstitial sites before the octahedral sites are fully occupied according to the existing experimental data (Ikuta et al., 2019).

From the difficulties discussed above, it is logical to use an averaged ΔV_H which includes both octahedral and tetrahedral H for FeH_x, as also noted by Antonov et al. (2019). Our partial occupancy models do not take into account the existence of multiples of configuration and disordering of H occupation expected for the real FeH_x, although they provide important insights for the energy differences between substitutions of H into different interstitial sites. Therefore, we chose to obtain ΔV_H from the FeH_3 model where both the octahedral and the tetrahedral sites are completely filled (Figure 3). The model yields: $\Delta V_H = 2.47$ Å^3/H at 0 GPa, which shows the best agreement with experimental estimation for FeH_x with both octahedral and tetrahedral H occupancies, 2.2 Å^3/H (Antonov et al., 2019; Ikuta et al., 2019) among our DFT models. Also, the DFT based estimation ($x = 1.1$) shows good agreement with the amount of H constrained by site occupancy from neutron diffraction (not by volume increase) by Ikuta et al. (2019) who estimated $x = 1$ for their data points at 12 GPa (the down-pointing triangles in Figure 3). From the model, we obtain $x = 1.84$ at 77 GPa for (Fe,Ni)H_x (Figure 3).

From our observation for the instability of the fcc phase with $x > 1$ (i.e., loss of H) during decompression and previous observation for predominantly $x = 1$ for FeH_x synthesized below melting temperature, we infer that the maximum H content possible for stable solid form of FeH_x is ∼1. If it is the case, our finding indicates that the liquid outer core has approximately 1.8 times greater H storage capacity than the solid inner core. We cannot also rule out the possibility of some loss of H during temperature quench in our experiments. In this case, the value of $x = 1.8$ reported here for liquid (Fe,Ni)H_x should be regarded as a lower bound of x for the liquid. We note that the experimental design here is to measure the maximum H storage capacity of (Fe,Ni)H_x liquid, not the partitioning of H between the liquid and solid Fe alloys, which is more proper to consider for estimating H contents in the liquid and solid parts of the cores when H amount is limited, such as terrestrial planets including Earth.

3.3. Effect of Ni on H Storage in Fe Alloy

Despite the fact that both (Fe,Ni)H_x and FeH_x above 77 GPa were heated above the projected melting temperature, we found much greater volume increase for the Ni-bearing alloy and therefore more H contained in the frozen form: $x = 1.84$ for $(Fe,Ni)H_x$ and $x = 1.69$ for FeH_x. It is possible that a small amount of Ni may reduce loss of H when Fe alloy converts from liquid to solid. To get more insight, we performed DFT calculations for the $FeH_{1.5}$ and $(Fe_{0.875}Ni_{0.125})H_{1.5}$ systems (Equation 1 and Figure S5 in Supporting Information S1). Our principal finding is that the incorporation of Ni lowers the formation enthalpy relative to $FeH_{1.5}$ over the entire pressure range. Near ambient pressure where the reference state of Fe is the bcc phase, the enthalpy of $(Fe_{0.875}Ni_{0.125})H_{1.5}$ is about 8 meV per formula unit lower than that of its $FeH_{1.5}$ counterpart while the relative enthalpy lowering of the Ni alloy is ~12 meV per formula unit at high pressures where the reference state of iron is hcp. The effect of Ni on enthalpy is much smaller near ~16 GPa where a cross over is found between the relative enthalpies compared to bcc/hcp Fe. This pressure is similar to the calculated bcc-hcp transition for pure iron (Mankovsky et al., 2013). The pressure dependence of the magnetic moment of the Ni alloy is about 10% lower than that of $FeH_{1.5}$ over the entire pressure range. Therefore, this energetics comparison can explain the observed larger amount of H in the fcc phase quenched from Fe liquid when Ni is present. We do not rule out the possibility of a small amount of Ni actually promotes the H solubility in Fe liquid at high pressure. It is desirable to explore this possibility in future studies.

4. Implications

Recent studies have shown that hydrogen becomes strongly siderophile and partitions into metallic iron over silicate melt at high pressures (Tagawa et al., 2021; Thompson et al., 2018; Yuan & Steinle-Neumann, 2020). The most important finding of our experiments is that the H storage capacity of Fe-Ni liquid is likely more than 1.8 times greater than that of the solid counterpart. The pressure range in this experiment overlaps with that expected for the magma ocean during the core formation (20–70 GPa), which likely determined the light element composition of the core. A recent study on temperature quenched hydrous silicate melt + iron liquid samples showed partitioning of H into the metallic liquid (Tagawa et al., 2021). In the experiments, because of H loss during pressure quench, the amount of H in Fe liquid was estimated from frozen form at 300 K and high pressures. We showed here that H storage capacity of Fe liquid is likely beyond the amount of H solid fcc can hold and some amount of H could be lost during temperature quench. This metastable behavior of the fcc phase quenched from liquid could therefore result in underestimation of the amount of H contained in $(Fe,Ni)H_x$ liquid at high temperatures. It has also been shown that H_2, instead of H_2O, can directly ingass to silicate magma at high pressures (Hirschmann et al., 2012). From the observation, ingassing of nebular hydrogen was proposed for the early Earth (Olson & Sharp, 2018). Our study suggests that large ingassing of hydrogen through alloying with liquid metal Fe is also possible during the formation of Earth. Another important implication is that the liquid outer core would likely have a larger H storage capacity than the solid inner core. Given partitioning behavior of H between silicate melt and iron liquid, it is likely that the liquid outer core may have the largest storage capacity for H in the Earth and the rocky planets. We note, however, that this issue should be ultimately addressed by partitioning experiments under limited amount of H reasonable for the Earth.

Many sub-Neptunes in the extrasolar systems are believed to have thick hydrogen atmosphere interfacing the magma ocean at tens of GPa's of pressure (Kite et al., 2019). Hydrogen can make the environment strongly reducing, stripping Fe from silicate melt to form a separate Fe liquid: $FeO + (x + 2)/2\ H_2 \rightarrow FeH_x + H_2O$ (Horn et al., 2023). Furthermore, Fe metal droplets in the magma ocean can be directly hydrogenated by ingassed H_2 (Hirschmann et al., 2012): $Fe + x/2H_2 \rightarrow FeH_x$. Such metallic liquid structures in the magma ocean will eventually sink toward the deep interior because of their high density, resulting in significant hydrogen ingassing in exoplanets of common type. Recent experiments have shown that Fe-H alloys can form from reaction between iron metal and water at high pressures: $3Fe + H_2O \rightarrow 2FeH + FeO$ (Ohtani et al., 2005). Therefore, water-rich planets (Zeng et al., 2019) could have a large amount of hydrogen stored in the metal during their core formation as well. For gas giants, the hydrogen-core interface would be at much higher pressures and therefore application of the results presented here should be made with care. However, a DFT study showed that Fe and H remain soluble in each other at pressures between 400 and 4,000 GPa (Wahl et al., 2013). Therefore, a significant amount of H stored in the core could be common for a large population of planets in our galaxy, from rocky planets to sub-Neptunes and gas giants.

Conflict of Interest

The authors declare no conflicts of interest relevant to this study.

Data Availability Statement

The data from experiments and density functional theory in this study are available at Zenodo via https://doi.org/10.5281/zenodo.7662676. A Python code to calculate the hydrogen content in (Fe,Ni)H_x using the density functional theory calculation is also included in a Jupyter notebook file in the repository.

Acknowledgments
We thank six anonymous reviewers for their helpful comments. The work has been supported by the NASA (80NSSC18K0353) and NSF (EAR1921298 and AST2005567). H.P., P.B., and S.-H.S. were supported partially by the Keck Foundation (PI: P. Buseck). The results reported herein benefit from collaborations and information exchange within NASA's Nexus for Exoplanet System Science (NExSS) research coordination network sponsored by NASA's Science Mission Directorate. A.V.G.C. gratefully acknowledges ASU's supercomputing resources. B.C. acknowledges the support from NSF (EAR-1555388, EAR-1829273). The synchrotron experiments were conducted at GeoSoilEnviroCARS (University of Chicago, Sector 13), Advanced Photon Source (APS). GeoSoilEnviroCARS is supported by the NSF-Earth Science (EAR-1634415) and DOE-GeoScience (DE-FG02-94ER14466). APS is supported by DOE-BES under contract DE-AC02-06CH11357.

References

Antonov, V. E. (2002). Phase transformations, crystal and magnetic structures of high-pressure hydrides of *d*-metals. *Journal of Alloys and Compounds*, *330*, 110–116. https://doi.org/10.1016/s0925-8388(01)01532-8

Antonov, V. E., Gurev, V. M., Kulakov, V. I., Kuzovnikov, M. A., Sholin, I. A., & Zuykova, V. Y. (2019). Solubility of deuterium and hydrogen in fcc iron at high pressures and temperatures. *Physical Review Materials*, *3*(11), 113604. https://doi.org/10.1103/PhysRevMaterials.3.113604

Badding, J. V., Hemley, R., & Mao, H. (1991). High-pressure chemistry of hydrogen in metals: In situ study of iron hydride. *Science*, *253*(5018), 421–424. https://doi.org/10.1126/science.253.5018.421

Binns, J., Donnelly, M.-E., Wang, M., Hermann, A., Gregoryanz, E., Dalladay-Simpson, P., & Howie, R. T. (2018). Synthesis of Ni_2H_3 at high temperatures and pressures. *Physical Review B*, *98*(14), 140101. https://doi.org/10.1103/physrevb.98.140101

Birch, F. (1947). Finite elastic strain of cubic crystals. *Physical Review*, *71*(11), 809–824. https://doi.org/10.1103/physrev.71.809

Birch, F. (1964). Density and composition of mantle and core. *Journal of Geophysical Research*, *69*(20), 4377–4388. https://doi.org/10.1029/jz069i020p04377

Deemyad, S., Sterer, E., Barthel, C., Rekhi, S., Tempere, J., & Silvera, I. F. (2005). Pulsed laser heating and temperature determination in a diamond anvil cell. *Review of Scientific Instruments*, *76*(12), 125104. https://doi.org/10.1063/1.2140493

Dorogokupets, P. I., Dymshits, A. M., Litasov, K. D., & Sokolova, T. S. (2017). Thermodynamics and equations of state of iron to 350 GPa and 6000 K. *Scientific Reports*, *7*(1), 41863. https://doi.org/10.1038/srep41863

Fu, S., Chariton, S., Prakapenka, V. B., & Shim, S.-H. (2023). Core origin of seismic velocity anomalies at Earth's core–mantle boundary. *Nature*. https://doi.org/10.1038/s41586-023-05713-5

Goncharov, A. F., Prakapenka, V. B., Struzhkin, V. V., Kantor, I., Rivers, M. L., & Dalton, D. A. (2010). X-ray diffraction in the pulsed laser heated diamond anvil cell. *Review of Scientific Instruments*, *81*(11), 113902. https://doi.org/10.1063/1.3499358

Hirose, K., Tagawa, S., Kuwayama, Y., Sinmyo, R., Morard, G., Ohishi, Y., & Genda, H. (2019). Hydrogen limits carbon in liquid iron. *Geophysical Research Letters*, *46*(10), 5190–5197. https://doi.org/10.1029/2019gl082591

Hirschmann, M., Withers, A., Ardia, P., & Foley, N. (2012). Solubility of molecular hydrogen in silicate melts and consequences for volatile evolution of terrestrial planets. *Earth and Planetary Science Letters*, *345–348*, 38–48. https://doi.org/10.1016/j.epsl.2012.06.031

Horn, H. W., Prakapenka, V., Chariton, S., Speziale, S., & Shim, S.-H. (2023). Reaction between hydrogen and ferrous/ferric oxides at high pressures and high temperatures—Implications for sub-Neptunes and super-Earths. *The Planetary Science Journal*, *4*(2), 30. https://doi.org/10.3847/psj/acab03

Ikuta, D., Ohtani, E., Sano-Furukawa, A., Shibazaki, Y., Terasaki, H., Yuan, L., & Hattori, T. (2019). Interstitial hydrogen atoms in face-centered cubic iron in the Earth's core. *Scientific Reports*, *9*(1), 7108. https://doi.org/10.1038/s41598-019-43601-z

Kato, C., Umemoto, K., Ohta, K., Tagawa, S., Hirose, K., & Ohishi, Y. (2020). Stability of fcc phase FeH to 137 GPa. *American Mineralogist*, *105*(6), 917–921. https://doi.org/10.2138/am-2020-7153

Kite, E. S., FegleyJr., B., Schaefer, L., & Ford, E. B. (2019). Superabundance of exoplanet sub-Neptunes explained by fugacity crisis. *The Astrophysical Journal Letters*, *887*(2), L33. https://doi.org/10.3847/2041-8213/ab59d9

Kresse, G., & Furthmüller, J. (1996). Efficient iterative schemes for ab initio total-energy calculations using a plane-wave basis set. *Physical Review B*, *54*(16), 11169–11186. https://doi.org/10.1103/physrevb.54.11169

Kresse, G., & Joubert, D. (1999). From ultrasoft pseudopotentials to the projector augmented-wave method. *Physical Review B*, *59*(3), 1758–1775. https://doi.org/10.1103/physrevb.59.1758

Mankovsky, S., Polesya, S., Ebert, H., Bensch, W., Mathon, O., Pascarelli, S., & Minár, J. (2013). Pressure-induced bcc to hcp transition in Fe: Magnetism-driven structure transformation. *Physical Review B*, *88*(18), 184108. https://doi.org/10.1103/physrevb.88.184108

Mao, W., Campbell, A. J., Heinz, D. L., & Shen, G. (2006). Phase relations of Fe–Ni alloys at high pressure and temperature. *Physics of the Earth and Planetary Interiors*, *155*(1–2), 146–151. https://doi.org/10.1016/j.pepi.2005.11.002

McDonough, W. (2003). 3.16–compositional model for the Earth's core. *Treatise on Geochemistry*, *2*, 547–568.

Narygina, O., Dubrovinsky, L. S., McCammon, C. A., Kurnosov, A., Kantor, I. Y., Prakapenka, V. B., & Dubrovinskaia, N. A. (2011). X-ray diffraction and Mössbauer spectroscopy study of fcc iron hydride FeH at high pressures and implications for the composition of the Earth's core. *Earth and Planetary Science Letters*, *307*(3–4), 409–414. https://doi.org/10.1016/j.epsl.2011.05.015

Ohta, K., Suehiro, S., Hirose, K., & Ohishi, Y. (2019). Electrical resistivity of fcc phase iron hydrides at high pressures and temperatures. *Comptes Rendus Geoscience*, *351*(2–3), 147–153. https://doi.org/10.1016/j.crte.2018.05.004

Ohtani, E., Hirao, N., Kondo, T., Ito, M., & Kikegawa, T. (2005). Iron-water reaction at high pressure and temperature, and hydrogen transport into the core. *Physics and Chemistry of Minerals*, *32*(1), 77–82. https://doi.org/10.1007/s00269-004-0443-6

Olson, P., & Sharp, Z. D. (2018). Hydrogen and helium ingassing during terrestrial planet accretion. *Earth and Planetary Science Letters*, *498*, 418–426. https://doi.org/10.1016/j.epsl.2018.07.006

Pépin, C., Dewaele, A., Geneste, G., Loubeyre, P., & Mezouar, M. (2014). New iron hydrides under high pressure. *Physical Review Letters*, *113*(26), 265504. https://doi.org/10.1103/physrevlett.113.265504

Pépin, C., Geneste, G., Dewaele, A., Mezouar, M., & Loubeyre, P. (2017). Synthesis of FeH_5: A layered structure with atomic hydrogen slabs. *Science*, *357*(6349), 382–385. https://doi.org/10.1126/science.aan0961

Perdew, J. P., Burke, K., & Ernzerhof, M. (1996). Generalized gradient approximation made simple. *Physical Review Letters*, *77*(18), 3865–3868. https://doi.org/10.1103/physrevlett.77.3865

Piet, H., Chizmeshya, A. V. G., Chen, B., Chariton, S., Greenberg, E., Prakapenka, V. B., & Shim, S.-H. (2021). Effect of nickel on the high-pressure phases in FeH. *Physical Review B*, *104*(22), 224106. https://doi.org/10.1103/PhysRevB.104.224106

Poirier, J.-P. (1994). Light elements in the Earth's outer core: A critical review. *Physics of the Earth and Planetary Interiors*, *85*(3–4), 319–337. https://doi.org/10.1016/0031-9201(94)90120-1

Prescher, C., & Prakapenka, V. B. (2015). DIOPTAS: A program for reduction of two-dimensional X-ray diffraction data and data exploration. *High Pressure Research*, *35*(3), 223–230. https://doi.org/10.1080/08957959.2015.1059835

Sagatova, D., Gavryushkin, P., Sagatov, N., Medrish, I., & Litasov, K. (2020). Phase diagrams of iron hydrides at pressures of 100–400 GPa and temperatures of 0–5000 K. *JETP Letters*, *111*(3), 145–150. https://doi.org/10.1134/s0021364020030108

Sakamaki, K., Takahashi, E., Nakajima, Y., Nishihara, Y., Funakoshi, K., Suzuki, T., & Fukai, Y. (2009). Melting phase relation of FeHx up to 20 GPa: Implication for the temperature of the earth's core. *Physics of the Earth and Planetary Interiors*, *174*(1–4), 192–201. https://doi.org/10.1016/j.pepi.2008.05.017

Seager, S., & Deming, D. (2010). Exoplanet atmospheres. *Annual Review of Astronomy and Astrophysics*, *48*(1), 631–672. https://doi.org/10.1146/annurev-astro-081309-130837

Shibazaki, Y., Terasaki, H., Ohtani, E., Tateyama, R., Nishida, K., Funakoshi, K.-I., & Higo, Y. (2014). High-pressure and high-temperature phase diagram for $Fe_{0.9}Ni_{0.1}$–H alloy. *Physics of the Earth and Planetary Interiors*, *228*, 192–201. https://doi.org/10.1016/j.pepi.2013.12.013

Shim, S.-H. (2017). PeakPo—A python software for X-ray diffraction analysis at high pressure and high temperature. https://doi.org/10.5281/zenodo.810200

Tagawa, S., Gomi, H., Hirose, K., & Ohishi, Y. (2022). High-temperature equation of state of FeH: Implications for hydrogen in Earth's inner core. *Geophysical Research Letters*, *49*(5), e2021GL096260. https://doi.org/10.1029/2021GL096260

Tagawa, S., Ohta, K., Hirose, K., Kato, C., & Ohishi, Y. (2016). Compression of Fe–Si–H alloys to core pressures. *Geophysical Research Letters*, *43*(8), 3686–3692. https://doi.org/10.1002/2016gl068848

Tagawa, S., Sakamoto, N., Hirose, K., Yokoo, S., Hernlund, J., Ohishi, Y., & Yurimoto, H. (2021). Experimental evidence for hydrogen incorporation into Earth's core. *Nature Communications*, *12*(1), 2588. https://doi.org/10.1038/s41467-021-22035-0

Thompson, E., Davis, A., Bi, W., Zhao, J., Alp, E., Zhang, D., et al. (2018). High-pressure geophysical properties of fcc phase FeH_X. *Geochemistry, Geophysics, Geosystems*, *19*(1), 305–314. https://doi.org/10.1002/2017gc007168

Toby, B., & Von Dreele, R. (2013). GSAS-II: The genesis of a modern open-source all purpose crystallography software package. *Journal of Applied Crystallography*, *46*(2), 544–549. https://doi.org/10.1107/s0021889813003531

Wahl, S. M., Wilson, H. F., & Militzer, B. (2013). Solubility of iron in metallic hydrogen and stability of dense cores in giant planets. *The Astrophysical Journal*, *773*(2), 95. https://doi.org/10.1088/0004-637x/773/2/95

Ye, Y., Prakapenka, V., Meng, Y., & Shim, S.-H. (2017). Intercomparison of the gold, platinum, and MgO pressure scales up to 140 GPa and 2500 K. *Journal of Geophysical Research: Solid Earth*, *122*(5), 3450–3464. https://doi.org/10.1002/2016jb013811

Ying, J., Liu, H., Greenberg, E., Prakapenka, V. B., & Struzhkin, V. V. (2018). Synthesis of new nickel hydrides at high pressure. *Physical Review Materials*, *2*(8), 085409. https://doi.org/10.1103/physrevmaterials.2.085409

Yuan, L., & Steinle-Neumann, G. (2020). Strong sequestration of hydrogen into the Earth's core during planetary differentiation. *Geophysical Research Letters*, *47*(15), e2020GL088303. https://doi.org/10.1029/2020gl088303

Zeng, L., Jacobsen, S. B., Sasselov, D. D., Petaev, M. I., Vanderburg, A., Lopez-Morales, M., et al. (2019). Growth model interpretation of planet size distribution. *Proceedings of the National Academy of Sciences*, *116*(20), 9723–9728. https://doi.org/10.1073/pnas.1812905116

Zhang, D., Jackson, J. M., Zhao, J., Sturhahn, W., Alp, E. E., Hu, M. Y., et al. (2016). Temperature of Earth's core constrained from melting of Fe and $Fe_{0.9}Ni_{0.1}$ at high pressures. *Earth and Planetary Science Letters*, *447*, 72–83. https://doi.org/10.1016/j.epsl.2016.04.026